

# RSC Advances



This is an *Accepted Manuscript*, which has been through the Royal Society of Chemistry peer review process and has been accepted for publication.

*Accepted Manuscripts* are published online shortly after acceptance, before technical editing, formatting and proof reading. Using this free service, authors can make their results available to the community, in citable form, before we publish the edited article. This *Accepted Manuscript* will be replaced by the edited, formatted and paginated article as soon as this is available.

You can find more information about *Accepted Manuscripts* in the [Information for Authors](#).

Please note that technical editing may introduce minor changes to the text and/or graphics, which may alter content. The journal's standard [Terms & Conditions](#) and the [Ethical guidelines](#) still apply. In no event shall the Royal Society of Chemistry be held responsible for any errors or omissions in this *Accepted Manuscript* or any consequences arising from the use of any information it contains.

## Effect of preparation of Fe-Zr-K catalyst on the product distribution of CO<sub>2</sub> hydrogenation

Xiaojuan Su, Jianli Zhang\*, Subing Fan, Qingxiang Ma, Tian-Sheng Zhao\*

State Key Laboratory Cultivation Base of Natural Gas Conversion, College of Chemistry and Chemical Engineering, Ningxia University, Yinchuan 750021, People's Republic of China

### Abstract

The precursors of Fe-Zr-K catalysts were prepared by microwave assisted homogeneous precipitation followed by incipient wetness impregnation. Obtained mesoporous samples were shaped in small and uniform particles. After reduction, the catalyst showed high activity for CO<sub>2</sub> hydrogenation to selective production of light olefins superior to the catalyst by co-precipitation. Characterization indicated with Zr addition the reducibility, the surface basicity and the surface atomic composition of the samples changed as the Zr content varied. The CO<sub>2</sub> adsorption ability of the samples was increased while the samples became hard to reduce relating to the interaction between iron species and zirconia. In the case of using 5Fe-1Zr-K under selected conditions of 1000 h<sup>-1</sup>, 320 °C and 2MPa, the CO<sub>2</sub> conversion and the selectivity of C<sub>2</sub>-C<sub>4</sub> olefins reached 54.36% and 53.63%, respectively. The olefin/paraffin ratio in the C<sub>2</sub>-C<sub>4</sub> hydrocarbon product fraction reached 6.44. The selectivity of CO and C<sub>5</sub><sup>+</sup> hydrocarbons were 3% and 19.78%, respectively. The catalytic activity remained stable up to 92 h time-on-stream reaction.

**Keywords:** Microwave assist; Homogeneous precipitation; Fe-Zr-K; CO<sub>2</sub> hydrogenation; Light olefins

\* Correspondence authors: Email: zhaots@nxu.edu.cn; zhangjl@nxu.edu.cn

## 1. Introduction

Increase in CO<sub>2</sub> emissions alongside the industrialization and the resulting greenhouse effect have given rise to ever-increasing concerns about the disposal of CO<sub>2</sub>. The chemical transformation of CO<sub>2</sub> to chemicals as one of carbon recycling avenues has attracted durative interests [1-6].

Compared with the H<sub>2</sub>/CO<sub>2</sub>-methanol-to-olefins process, direct synthesis of light olefins from CO<sub>2</sub> hydrogenation avoids the methanol synthesis and is more cost-effective. Research suggested that CO<sub>2</sub> hydrogenation to light olefins proceeds in two steps: reduction of CO<sub>2</sub> to CO via the reverse water-gas shift (RWGS) reaction, followed by CO hydrogenation via Fisher-Tropsch (F-T) reaction [7-8] as follows:



Various iron-based catalysts have been studied for this direct process [9-21] because they are usually adopted in the industrial shift reaction as well as F-T reaction [22]. Catalyst's formulation and preparation procedure affect obviously their performance. Unpromoted iron-based catalysts exhibit high methane selectivity [9, 10, 19]. Introduction of potassium promoter shows enhancement to carburization of iron species, formation of iron carbide active phases [9] and to selectivity of light olefins [15, 19, 20]. Several structural supports and chemical promoters have been employed in order to improve the catalytic performance and to tailor the product distribution [11-18]. Manganese stabilizes the Fe-K catalyst due to higher resistance of bulk oxidation but doesn't change the product distribution [11]. Alumina supported Fe-K shows high conversion of CO<sub>2</sub> and low selectivity of CO and methane at reaction

temperature of 400 °C with the  $C_5^+$  selectivity above 33% [12].  $\gamma$ - $Al_2O_3$  supported Fe-Mn-K lowers the formation of methane and increases the product ratio of olefin/paraffin [17]. Zirconia supported K-Fe also displays higher selectivity of light olefins while the CO selectivity was 15% [23]. Up to now, the selectivity of CO and methane or one of them in  $CO_2$  hydrogenation still remains higher. Thus, further reducing these two side products is desired.

Based on the two-step reaction mechanism of  $CO_2$  hydrogenation to light olefins, the formation of CO or methane may be reduced by tuning the rates of the two reactions. The F-T rate and the WGS rate were indicated to be altered with water addition during F-T synthesis reaction [24]. A bifunctional catalyst of ceria modified Fe/Mn/K for olefin production from  $CO_2$  hydrogenation was reported with combining the RWGS and F-T chain growth activity [18]. Zirconia alone provides adsorption sites for the surface reaction intermediates and the catalytic behavior of metal/zirconia for  $CO_2$  hydrogenation is metal type dependent and influenced by the interfacial contact area between the metal and zirconia [25]. Methane formation is suppressed by  $H_2O$  in the WGS reaction over Rh/ $Fe_2O_3$ / $ZrO_2$  [26]. On the other hand, iron-based catalysts with higher surface area from the microemulsion technology exhibit higher activity for  $CO_2$  hydrogenation [14] and mesoporous  $xFeMnO$  by sol-gel process enhances  $CO_2$  hydrogenation to  $C_2$ - $C_5$  hydrocarbons [21]. With faster reaction rate than the conventional heating, microwave assisted-homogeneous precipitation has been shown the potential in obtaining catalyst materials with desirable properties as fine particles and good chemical homogeneity [27-28].

To further understand the role of Zr promoter in iron catalyst for CO<sub>2</sub> hydrogenation to light olefins, in this work Fe-Zr-K catalysts were prepared using microwave assisted-homogeneous precipitation followed by incipient wetness impregnation methods. The effects of Zr addition amount on the structural properties of the precursors of Fe-Zr-K catalysts and on the activity for CO<sub>2</sub> hydrogenation were investigated by means of physic-chemical characterization. The influencing mechanism of zirconia on iron catalysts in product selectivity and activity stability was correlated.

## 2. Experimental

### 2.1 Sample preparation

Fe-Zr sample was prepared by the microwave-assisted homogeneous precipitation (MAHP) method with urea as precipitator. The molar ratio of Fe/Zr included 7:1, 5:1, 3:1 and 1:1. The molar ratio of (Fe+Zr)/urea was 1:6. In the typical procedure, desired amounts of Fe(NO<sub>3</sub>)<sub>3</sub>·9H<sub>2</sub>O, ZrO(NO<sub>3</sub>)<sub>2</sub>·2H<sub>2</sub>O and urea were mixed in deionized water of 200 mL under stirring until complete dissolution. Then, the solution was transformed into a Teflon-lined sample holder and reacted at microwave conditions (2450 MHz, 500 W, 1.6 MPa, 170-180 °C) for 2 h. The product was separated via centrifugation, washed, dried at 120 °C overnight and calcined at 500 °C in air for 3 h. The sample without Zr addition was prepared using the same procedure. For comparison, Fe-Zr samples by co-precipitation with NH<sub>3</sub>·H<sub>2</sub>O as precipitator were also prepared and marked with suffix [C].

Fe-Zr-K sample was prepared by incipient wetness impregnation in a fixed Fe/K

molar ratio of 10:1. The aqueous solution with desired amount of  $K_2CO_3$  was impregnated on Fe-Zr sample, and then dried at 120 °C overnight. The obtained samples were named in turn as 7Fe-1Zr-K, 5Fe-1Zr-K, 3Fe-1Zr-K, 1Fe-1Zr-K, Fe-K and 5Fe-1Zr-K[C].

## 2.2 Sample characterization

X-ray powder diffraction (XRD) patterns were recorded on a Rigaku D/MAX 2200PCX diffractometer with Ni-filtered Cu  $K\alpha$  radiation at 40 kV and 30 mA at scanning speed of 8°/min.

Scanning electron microscopy (SEM) images were obtained on a JEOL-JSM-7500F microscope at 1kV.

$N_2$  physical adsorption-desorption isotherms were measured at -196 °C on a JW-BK132F instrument after sample was pretreated under vacuum at 300 °C for 2 h. The BET surface area was calculated from the adsorption branch. The mesopore and micropore parameter calculation was based on the BJH and HK models, respectively.

$H_2$  temperature-programmed reduction ( $H_2$ -TPR) measurements were carried out on a chemisorption analyzer (TP5000). In a typical procedure, sample (20-40 mesh) of 70 mg was pretreated in a quartz tube at 350 °C in He (25 mL/min) for 1 h and cooled to room temperature. Then the sample was reduced by a mixed gas composed of 5%  $H_2$  and 95%  $N_2$  as the temperature rose from room temperature to 800 °C at a heating rate of 10 °C/min. The  $H_2$  consumption was synchronously detected on a gas chromatography with thermal conductivity detector.

$CO_2$  temperature-programmed desorption ( $CO_2$ -TPD) was performed on the same

TP5000. 200 mg sample was pretreated at 400 °C for 3h in a flow of 30% H<sub>2</sub> and 70% N<sub>2</sub> (30 mL/min), and purged by He (25 mL/min) for 1 h. Then the sample was pulse-adsorbed by CO<sub>2</sub> at 50 °C until saturation, followed by He purge for 1h. Finally, the sample was heated in He (25 mL/min) as the temperature rose from room temperature to 800 °C at a heating rate of 10 °C/min. The CO<sub>2</sub> desorption amount was synchronously detected.

X-ray photoelectron spectra (XPS) were obtained on a Thermo SCIENTIFIC ESCALAB 250 equipped with a Al K $\alpha$  X-ray source ( $h\nu=1486.8$  eV) at 15 kV and 10 mA. The background vacuum of analysis room was  $2\times 10^{-9}$  mbar. The binding energies (BE) were calibrated using the C1s peak at 284.8 eV from adventitious carbon.

### 2.3 Catalytic activity evaluation

Activity tests were carried out in a flow type fixed-bed system with a stainless steel reactor (350 mm length  $\times$  8 mm i.d.  $\times$  12 mm o.d). Typical conditions were as follows: precursor packing amount=2 mL (20-40 mesh), H<sub>2</sub>/CO<sub>2</sub> (molar ratio)=3/1, GHSV=1000 h<sup>-1</sup>, T=320 °C and P=2.0 MPa. The sample was first reduced at 400 °C for 8 h by 30% H<sub>2</sub> in N<sub>2</sub> (GHSV=1000 h<sup>-1</sup> and P=0.1MPa). Then the feed gas was switched in, the reaction started and proceeded for 96 h time-on-stream (TOS). The sampling interval was 12 h. The data in Table 3 were obtained at TOS = 68 h. Effluent gas was analyzed on an on-line gas chromatograph (GC-9160), with a  $\phi 3$  mm  $\times$  2 m TDX-01 packed column for C<sub>1</sub> product analysis on TCD, and a 50 m  $\times$  0.53 mm  $\times$  40  $\mu$ m Al<sub>2</sub>O<sub>3</sub> capillary column for C<sub>1</sub>-C<sub>5</sub> hydrocarbon product analysis on FID,

respectively. Collected liquid products were analyzed on an off-line GC-9160, with a  $\phi 3 \text{ mm} \times 2 \text{ m}$  Porapak Q packed column for aqueous phase product analysis on TCD and a  $50 \text{ m} \times 0.32 \text{ mm} \times 1.0 \text{ }\mu\text{m}$  HJ-1 capillary column for oil phase product analysis on FID. The data after 48 h time-on-stream reaction were used for the activity discussion. The conversion of  $\text{CO}_2$  and the selectivity of products were calculated based on carbon balance.

$$\text{CO}_2 \text{ conv.} = (\text{F}_{\text{in}} \times y_{\text{in}}^{\text{CO}_2} - \text{F}_{\text{out}} \times y_{\text{out}}^{\text{CO}_2}) / (\text{F}_{\text{in}} \times y_{\text{in}}^{\text{CO}_2}) \times 100\%$$

$$\text{CH}_4(\text{CO}) \text{ sel.} = (\text{F}_{\text{out}} \times y_{\text{out}}^i) / (\text{F}_{\text{in}} \times y_{\text{in}}^{\text{CO}_2} \times \text{Conv. CO}_2) \times 100\%$$

where,  $\text{F}_{\text{in}}$  was the mole flow rate of the feed gas, mol/h;  $\text{F}_{\text{out}}$  was the mole flow rate of the effluent, mol/h;  $y_{\text{out}}^i$  was the mole fraction of  $\text{CH}_4$  (CO) in the effluent. Calculation for hydrocarbon product selectivity included gaseous phase and liquid phase products.

Chain growth probability ( $\alpha$ ) was calculated according to Anderson-Schulz-Flory model for the product distribution:  $\ln (W_n/n) = n \ln \alpha + \ln [(1-\alpha)^2/\alpha]$ , where  $n$  is the number of carbon atoms in a product;  $W_n$  is the weight fraction of corresponding product.

### 3. Results and discussion

#### 3.1 Phases of the samples

The XRD patterns of the samples are shown in Fig.1. The characteristic diffraction peaks at  $2\theta$  of  $24.2^\circ$ ,  $33.3^\circ$ ,  $35.7^\circ$ ,  $40.9^\circ$ ,  $49.6^\circ$ ,  $54.1^\circ$ ,  $62.6^\circ$  and  $64.1^\circ$  were ascribed to  $\alpha\text{-Fe}_2\text{O}_3$  phase [29] and those at  $2\theta$  of  $30.7^\circ$ ,  $51.2^\circ$  and  $60.8^\circ$  attributed to tetragonal  $\text{ZrO}_2$  phase [30].

For samples (a)-(e) before reduction and reaction, as the Zr content increased, the peak strength of  $\alpha$ -Fe<sub>2</sub>O<sub>3</sub> was gradually diminished while that of ZrO<sub>2</sub> increased. K impregnation did not obviously affect the phases as shown in samples (b) and (c). The diffraction peaks of  $\alpha$ -Fe<sub>2</sub>O<sub>3</sub> by the MAHP method were stronger than that by co-precipitation as shown in samples (b) and (d). For samples (f)-(h) after reaction, Fe<sub>3</sub>O<sub>4</sub> phase was observed via the diffraction peaks at  $2\theta$  of 18.34°, 30.18°, 36.56°, 43.24°, 53.54°, 57.10° and 62.74° while  $\alpha$ -Fe<sub>2</sub>O<sub>3</sub> phase disappeared, suggesting the iron species is transformed to Fe<sub>3</sub>O<sub>4</sub> [23, 31]. In contrast, ZrO<sub>2</sub> phase did not change distinctly before and after reaction.

The average crystal particle sizes of  $\alpha$ -Fe<sub>2</sub>O<sub>3</sub> phase in the samples by XRD results are shown in Table 1. As the Zr content increased, the particle of  $\alpha$ -Fe<sub>2</sub>O<sub>3</sub> crystal phase, corresponding to the (104) crystal face, increased first and then decreased. With the MAHP preparation method, the crystal particle of  $\alpha$ -Fe<sub>2</sub>O<sub>3</sub> phase in 5Fe-1Zr sample was 28.1 nm, without significant change compared with 24.0 nm of 5Fe-1Zr [C] by co-precipitation.

**Table 1 Crystal particle of  $\alpha$ -Fe<sub>2</sub>O<sub>3</sub> phase**

Sample	Size/nm
Fe <sub>2</sub> O <sub>3</sub>	24.9
7Fe-1Zr	32.7
5Fe-1Zr	28.1
3Fe-1Zr	24.0
1Fe-1Zr	11.1
5Fe-1Zr[C]	24.0

### 3.2 Textural properties of the samples

To check the effect of the MAHP method on preparation, the SEM photographs of fresh samples prepared by the MAHP before K impregnation were taken as shown in Fig.2. Samples (a)-(c) were shaped in small and uniform particles. The microscopic morphology particle size was in the range of 50-60 nm. In contrast, sample (d) prepared by co-precipitation showed large and irregular particles. During the MAHP, the OH<sup>-</sup> ions required for precipitation were gradually released by the hydrolysis of urea, or the pH value maintained consistent. Besides, the hydrothermal temperature reached 170-180 °C, the nucleation might be faster than the crystal particle growth. These two conditions cause the formation of small and uniform particles [32].

The N<sub>2</sub> adsorption-desorption isotherms of fresh samples before K impregnation are shown in Fig.3. Samples (a)-(e) prepared by the MAHP method showed the type IV isotherm pattern with H<sub>3</sub>-type hysteresis loop, indicating the mesopores in the samples [21].

The pore parameters of fresh samples before reduction and reaction are summarized in Table 2. As the Zr content increased, the surface area and the micropore volume increased. The mesopore volumes of all samples were much larger than the micropore volumes and 5Fe-1Zr-K and 3Fe-1Zr-K showed the maximal mesopore volume. Besides, 5Fe-1Zr-K had the minimal mesopore diameter while 1Fe-1Zr-K had the maximal mesopore diameter. By contrast, 5Fe-1Zr-K[C] prepared by co-precipitation had the largest surface area, micropore volume and larger mesopore volume, mesopore diameter.

**Table 2 Pore parameters of the samples**

Samples	Surface area (m <sup>2</sup> /g)	Mesopore volume (cm <sup>3</sup> /g)	Micropore volume (cm <sup>3</sup> /g)	Mesopore diameter (nm)
Fe-K	22.1	0.092	0.008	2.54
7Fe-1Zr-K	39.7	0.156	0.014	2.31
5Fe-1Zr-K	52.6	0.190	0.020	2.25
3Fe-1Zr-K	76.7	0.191	0.029	11.58
1Fe-1Zr-K	83.5	0.168	0.032	11.94
5Fe-1Zr-K[C]	95.3	0.153	0.037	7.32

### 3.3 Reduction behavior of the samples

From H<sub>2</sub>-TPR profiles of the samples in Fig.4, it can be seen that all fresh samples produced two reduction peaks.

For Fe<sub>2</sub>O<sub>3</sub> (a), the sharp peak at 280-420 °C and broad one at 450-800 °C, were assigned to the initial reduction of α-Fe<sub>2</sub>O<sub>3</sub> to Fe<sub>3</sub>O<sub>4</sub> and then the reduction of Fe<sub>3</sub>O<sub>4</sub> to α-Fe, respectively [31]. For Fe-K (b), two peaks appeared at low temperatures were ascribed to the reduction of α-Fe<sub>2</sub>O<sub>3</sub> to Fe<sub>3</sub>O<sub>4</sub> and partial Fe<sub>3</sub>O<sub>4</sub> to FeO [13]. For K-containing samples (b)-(g), the first peaks shifted to high temperatures, suggesting that K modification causes the reduction hard. K promoter has also been proved to suppress the adsorption of H<sub>2</sub> to a certain extent [12, 23]. Besides, the second peaks of 7Fe-1Zr-K (c) and 5Fe-1Zr-K (d) shifted to high temperatures, indicating the inhibition effect on the reduction of Fe<sub>2</sub>O<sub>3</sub> and the formation of iron phase through FeO phase. With increasing the Zr content in samples (f) and (g), the second peak shifted to lower temperatures, which is coincident with the reported results that Zr

addition improves the dispersion of iron phases and makes iron species easily reduced [33]. These results demonstrate that there exists the interaction between iron species and zirconia and it was the strongest in 5Fe-1Zr-K. The reducibility of sample 5Fe-1Zr-K[C] by co-precipitation was different from that by the MAHP method. Similar to Fe-K (b), two reduction peaks appeared at low temperatures for 5Fe-1Zr-K[C] (e). The second peak was at 500-650 °C, lower than that of corresponding 5Fe-1Zr-K, implying the reduction of  $\text{Fe}_3\text{O}_4$  to  $\alpha\text{-Fe}$  is relatively easy.

### 3.4 Surface adsorption behavior of the samples

Fig.5 shows the  $\text{CO}_2$ -TPD profiles of fresh samples after the  $\text{H}_2$  pretreatment but before reaction. Sample Fe-K (a) appeared two  $\text{CO}_2$  desorption peaks at 120 °C-170 °C and 610 °C-800 °C. After addition of Zr, the peak slightly shifted to high temperatures and the  $\text{CO}_2$  desorption amount increased as shown for sample (b). In addition, two new desorption peaks appeared at 200 °C-320 °C and 510 °C-620 °C. These data suggest that the adsorption of  $\text{CO}_2$ , which is related to surface basicity [12], is intensified due to the  $\text{ZrO}_2$  formation by Zr addition. With further addition of Zr in sample (d), the high temperature desorption peak dramatically decreased. By comparison, the high temperature desorption peak strength of 5Fe-1Zr-K[C] (c) showed weaker since the desorption peak temperature was lower.

### 3.5 Surface composition of the samples

The XPS spectra of fresh samples before reduction and reaction are shown in Fig. 6. For all samples in Fig.6-A, the binding energy (BE) at 710.9 eV and 724.5 eV was ascribed to  $\text{Fe}(2p_{3/2})$  and  $\text{Fe}(2p_{1/2})$ , respectively. The satellite peak at 718.9 eV

characterized the existence of  $\text{Fe}_2\text{O}_3$  [21]. In Fig.6-B, the BE at 182.1 eV was attributed to  $\text{Zr}(3d_{5/2})$  of  $\text{ZrO}_2$ . K addition in Fig. 6A (b) caused a slight decrease in the BE of  $\text{Fe}(2p_{1/2})$  compared with  $\text{Fe}_2\text{O}_3$  (a). It was proposed that K lowers the metal work function by donating electron to the vacant d orbits of the iron, enhancing the dissociative adsorption of CO while lowering the  $\text{H}_2$  adsorption ability [34]. Furthermore, the BE of  $\text{Fe}(2p_{3/2})$  and  $\text{Zr}(3d_{5/2})$  were lowered for the Fe-Zr samples in Fig.6-A (c)-(e) and in Fig.6-B (a)-(c), indicating the increased interaction between iron species and zirconia.

It can be seen from Fig.7 that after reaction the BE of  $\text{Fe}(2p_{3/2})$  in 5Fe-1Zr-K shifted slightly towards low energy compared with those before reduction and reaction, suggesting the existence of  $\text{Fe}_3\text{O}_4$  in accordance with the XRD results. The binding energy of carbon species in 5Fe-1Zr-K sample is shown in Fig.8. Before and after reaction, there was carbon (C1s, BE: 284.8 eV) on the sample surface while carbidic carbon (BE: 283.1-283.4 eV) [21] was not observed. This suggests that the carburization of Fe probably occur during the reaction and after reaction the Fe species transform to iron oxides.

From the atomic concentration of the XPS spectra, the atomic Zr/Fe ratios of the samples were calculated. As shown in Fig.9, the calculated Zr/Fe ratios are higher than the preparation ratios, revealing that Zr is enriched on the sample surface and the enrichment is stronger on 5Fe-1Zr [C] than on 5Fe-1Zr.

### 3.6 Catalytic activity for $\text{CO}_2$ hydrogenation

The catalytic activity of the samples for  $\text{CO}_2$  hydrogenation at selected conditions

is shown in Table 3. It can be seen that all samples prepared by the MAHP method showed higher activity with CO<sub>2</sub> conversion above 43%. The main products were hydrocarbons except for CO and small amount of oxygenates. 5Fe-1Zr-K sample displayed the maximum CO<sub>2</sub> conversion of 54.36%. In addition to presenting uniform particles with better dispersion, 5Fe-1Zr-K had the strongest surface basicity as the CO<sub>2</sub>-TPD profile shows in Fig.5, which should be favorable for the CO<sub>2</sub> adsorptive activation and conversion.

In the production distribution, the CH<sub>4</sub> selectivity over Fe-K was lower than that over Fe-Zr-K but the CO and C<sub>5</sub><sup>+</sup> selectivity were high. As the Zr content increased, the CH<sub>4</sub> selectivity was gradually increased while the C<sub>5</sub><sup>+</sup> selectivity decreased, indicating that the Zr addition in the catalyst samples suppresses the formation of the C<sub>5</sub><sup>+</sup> (heavy) products. As the Fe/Zr ratio increased, the CO<sub>2</sub> conversion and the selectivity of light olefins (C<sub>2</sub><sup>=</sup>-C<sub>4</sub><sup>=</sup>) first increased and then decreased. At the Fe/Zr ratio of 5, the CO<sub>2</sub> conversion and the C<sub>2</sub><sup>=</sup>-C<sub>4</sub><sup>=</sup> selectivity reached the maxima of 54.36% and 53.63%, respectively. Meantime, the selectivity of CO was the lowest (3%). The O/P ratio in the C<sub>2</sub>-C<sub>4</sub> hydrocarbon products was 6.44. In consideration of the interaction between iron species and zirconia indicated by the aforementioned XPS results (Fig.6) as well as the H<sub>2</sub>-TPR results (Fig.4), it is likely that during reduction of the samples, zirconia would also lower metal work function by donating electron to iron and enhance the adsorption of CO while reducing the H<sub>2</sub> adsorption, resulting in an increase in the light olefin products.

By contrast, 5Fe-1Zr-K[C] catalyst prepared by co-precipitation showed the lowest

CO<sub>2</sub> conversion although better product distribution. As shown in Fig.9, Zr tended to more enrichment on the catalyst surface prepared by co-precipitation. This enrichment might reduce the active site number on the catalyst surface, influencing the Fe-Zr interaction and the catalytic activity. Furthermore, weaker surface basicity of 5Fe-1Zr-K[C] than that of 5Fe-1Zr-K (see Fig. 5) was unfavorable for the CO<sub>2</sub> adsorptive activation.

**Table 3 Catalytic activity of the samples for CO<sub>2</sub> hydrogenation**

Catalysts	CO <sub>2</sub> Conv. /%	Sel. /%			Hydrocarbon distribution <sup>c</sup> /C%				O/P
		CO	HC <sup>a</sup>	Oxy. <sup>b</sup>	CH <sub>4</sub>	C <sub>2</sub> <sup>=</sup> -C <sub>4</sub> <sup>=</sup>	C <sub>2</sub> <sup>0</sup> -C <sub>4</sub> <sup>0</sup>	C <sub>5</sub> <sup>+</sup>	
Fe-K	48.33	7.45	89.17	3.38	16.12	50.53	6.69	26.67	7.55
7Fe-1Zr-K	49.78	7.10	91.84	1.06	19.62	52.70	8.45	19.21	6.24
5Fe-1Zr-K	54.36	3.00	96.58	0.42	19.78	53.63	8.33	18.26	6.44
3Fe-1Zr-K	51.55	6.16	90.39	3.45	21.77	50.61	9.94	17.68	5.09
1Fe-1Zr-K	43.43	9.88	90.11	0.01	24.74	46.61	14.20	14.46	3.28
5Fe-1Zr-K[C]	34.02	4.47	94.61	0.92	19.74	48.82	7.92	23.51	6.17

Reaction conditions: H<sub>2</sub>/CO<sub>2</sub> = 3/1, GHSV = 1000 h<sup>-1</sup>, 2MPa, 320 °C.

a HC: hydrocarbons.

b Oxy.: oxygenates.

c C<sub>2</sub><sup>=</sup>-C<sub>4</sub><sup>=</sup>: C<sub>2</sub>-C<sub>4</sub> olefins; C<sub>2</sub><sup>0</sup>-C<sub>4</sub><sup>0</sup>: C<sub>2</sub>-C<sub>4</sub> paraffins; C<sub>5</sub><sup>+</sup>: C<sub>5</sub><sup>+</sup> hydrocarbons.

It has been reported that the steady state establishment of F-T synthesis over iron catalysts can be divided into five episodes of distinct kinetic regimes, which lasts about 60 h. As the reaction time extends, Fe species undergo transformation from iron oxide to iron carbide (Fe<sub>5</sub>C<sub>2</sub>) [35].

Fig.10 shows the the catalytic activity of CO<sub>2</sub> hydrogenation over 5Fe-1Zr-K and

the production change at set reaction conditions as time-on-stream. It is clear that the catalytic activity exhibited an induction period of about 60 h. At the initial reaction stage, the CO<sub>2</sub> conversion tended to increase as the active phase iron carbide was gradually formed. After 60 h, both the CO<sub>2</sub> conversion and the C<sub>2</sub><sup>=</sup>-C<sub>4</sub><sup>=</sup> selectivity remained above 55% and 53% respectively. The CO selectivity retained at 3% from the incipient about 8%. As the preceding characterization indicates there exists the interaction between iron species and zirconia, this might play a stable role in the active phase of catalysts [26].

Chain growth probability ( $\alpha$ ) for CO<sub>2</sub> hydrogenation over the catalyst samples is shown in Fig. 11. With Zr addition, the  $\alpha$  tends to decrease. As the Zr content increases, the  $\alpha$  decreases from 0.64 over Fe-K to 0.53 over 1Fe-1Zr-K. This is well in accordance with the hydrocarbon product distribution in Table 3. That is, CH<sub>4</sub> increases while C<sub>5</sub><sup>+</sup> hydrocarbons decrease. The  $\alpha$  over 5Fe-1Zr-K[C] is higher than that over 5Fe-1Zr-K, the formation of C<sub>5</sub><sup>+</sup> is more. Moreover, the  $\ln(W_n/n)$  values for C<sub>2</sub> hydrocarbons show negative deviation to the fitted line. As the  $\alpha$  decreases, the deviation tends to diminish, implying the secondary reactions of C<sub>2</sub> towards heavy products are likely suppressed.

These results demonstrate that certain amount addition of Zr in Fe-K by the MAHP method, on the one hand, can improve the dispersion of active Fe on the uniform catalyst particles during the course of reduction/reaction and promote the uptake and activation of CO<sub>2</sub> by increasing the surface basicity on the catalyst surface. On the other hand, the Fe-Zr interaction shows positive effect to stabilize the catalysts. The

CO<sub>2</sub> hydrogenation activity towards light olefins is thus improved.

#### 4. Conclusion

The precursors of Fe-Zr-K catalysts prepared by microwave-assisted homogeneous precipitation method showed small and uniform particles and better dispersion of iron species. After reduction they showed high activity for hydrogenation of CO<sub>2</sub> to light olefins. Appropriate amount addition of Zr promoter and K modification can increase the catalyst surface basicity and the interaction between iron species and zirconia, resulting significant improvement in the CO<sub>2</sub> conversion and the product distribution. When the Fe/Zr ratio was 5, the CO<sub>2</sub> conversion and the light olefins selectivity reached the maxima with the highest O/P ratio in C<sub>2</sub>-C<sub>4</sub> hydrocarbon product fraction. Meantime the selectivity of CO was reduced as low as 3%. After the induction period the catalyst remained stable up to 92 h time-on-stream reaction.

The activity stability is possibly due to strong.

#### Acknowledgements

Financial supports from Special Prophase Project on Basic Research of Department of Science and Technology of China (Grant No.2012CB723106) and Natural Science Foundation of China (Grant No.21366025) are greatly acknowledged.

#### References

- [1] M Mikkelsen, M Jørgensen and F C Krebs, *Energy Environ. Sci.*, 2010, **3**, 43-81.
- [2] R W Dorner, D R Hardy, F W Williams and H D Willauer, *Energy Environ. Sci.*, 2010, **3**, 884-890.

- [3] W Wang, S Wang, X Ma and J Gong, *Chem. Soc. Rev.*, 2011, **40**, 3703-3727.
- [4] M He, Y Sun and B Han, *Angew. Chem. Int. Ed.*, 2013, **52**, 2-16.
- [5] G Centi, E A Quadrelli and S Perathoner, *Energy Environ. Sci.*, 2013, **6**, 1-19.
- [6] S Zhang, H Yan, M Wei, D G. Evans and X Duan, *RSC Adv.*, 2014, **4**, 30241-30249.
- [7] D Gordon, Weatherbee and C H Bartholomew, *J.Catal.*, 1984, **87**, 352-362.
- [8] T Riedel, G Schaub, K Jun and K Lee, *Ind. Eng.Chem. Res.*, 2001, **40**, 1355-1363.
- [9] M Lee, J Lee and C Chang, *Bull. Chem. Soc. Jpn.* 1989, **62**, 2756-2758.
- [10] M Lee, J Lee and C Chang, *J. Chem. Eng. Japan.*, 1990, **23**, 130-136.
- [11] J Lee, W Chern and M Lee, *Can. J. Chem. Eng.*, 1992, **70**, 511-515.
- [12] P H Choi, K Jun, S Lee, M J Choi and K W Lee, *Catal. Lett.*, 1996, **40**, 115-118.
- [13] G Kishan, M Lee, S Nam, M. Choi and K. Lee, *Catal. Lett.*, 1998, **56**, 215-219.
- [14] T Herranz, S Rojas, F JPérez-Alonso and J.L.G. Fierro, *Appl. Catal. A: Gen.*, 2006, **311**, 66-75.
- [15] J Kim, S Lee, S Lee, M. Choi and K. Lee, *Catal. Today*, 2006, **115**, 228-234.
- [16] P S Sai Prasad, J W Bae, K Jun and K W Lee, *Catal. Surv. Asia*, 2008, **12**, 170-183.
- [17] R W Dorner, D R Hardy, F W Williams and H D Willauer, *Appl. Catal. A: Gen.*, 2010, **373**, 112-121.
- [18] R W Dorner, D R Hardy, F W Williams and H D Willauer, *Catal. Commun.*, 2011, **15**, 88-92.
- [19] Z You, W Deng, Q Zhang and Y Wang, *Chin. J. Catal.*, 2013, **34**, 956-963.

- [20] M Martinelli, C G Visconti, L Lietti, P Forzatti, C Bassano and P Deiana, *Catal. Today*, 2014, **228**, 77-88.
- [21] M Al-Dossary, A A Ismail, J L G Fierro, H Bouzid and S A Al-Sayari, *Appl. Catal. B: Environ.*, 2015, **165**, 651-660.
- [22] Gerard P. Van Der Laan, A. A. C. M. Beenackers, *Catal. Rev. Sci. Eng.*, 1999, **41**, 255-318.
- [23] J Wang, Z You, Q Zhang, W. Deng, Y. Wang, *Catal. Today*, 2013, **215**, 186-193.
- [24] Rao Pendyala V R, Jacobs G, Mohandas J C, M Luo, W Ma, M K Gnanamani and B H Davis, *Appl. Catal. A: Gen.*, 2010, 389(1-2), 131-139.
- [25] J O R Wambach, A Baiker and A Wokaun, *Phys. Chem. Chem. Phys.*, 1999, **1**, 5071-5080.
- [26] A A Hakeem, R S. Vásquez, J Rajendran, M Li, R J. Berger, J J Delgado, F Kapteijn and M Makkee, *J. Catal.*, 2014, **313**, 34-45.
- [27] F. Bondioli, A.M. Ferrari, C. Leonelli, C. Siligardi and G.C. Pellacani, *J. Am. Ceram. Soc.*, 2001, **84**, 2728-2730.
- [28] Du J, Zhang Y, Tian T, S C Yan and H T Wang, *Mater. Res. Bull.*, 2009, **44**, 1347-1351.
- [29] Ş. özkara-Aydinoğlu, Ö. Ataç, Ö.F. Gül, Ş. Kınayyigit, S. Şal, M. Baranak and İ. Boz, *Chem. Eng. J.*, 2012, **181-182**, 581-589.
- [30] V G Deshmane and Y G Adewuyi, *Micropor. Mesopor. Mater.*, 2012, **148**, 88-100.
- [31] W Ning, N Koizumi, H Chang, T Mochizuki, T Itoh and M Yamada, *Appl. Catal.*

A: Gen., 2006, **312**, 35-44.

[32] J Baneshi, M Haghghi, N Jodeiri, M. Abdollahifar and H. Ajamein, Energy Convers. Manage., 2014, **87**, 928-937.

[33] K Chen, Y Fan and Q J Yan, Chin. J. Catal., 1995, **16**, 433-436.

[34] M E Dry, T Shingles, L J Boshoff and G J Oosthuizen, J. Catal., 1969, **15**, 190-199.

[35] H.Schulz, T. Riedel, G. Schaub, Topics in Catal., 2005, **32**, 117-124.

## Figure captions

### Fig.1 XRD patterns of the samples

(a)-(e): before reduction and reaction; (f)-(h): after reaction

### Fig.2 SEM photographs of the samples

(a) Fe<sub>2</sub>O<sub>3</sub> (b) 7Fe-1Zr (c) 5Fe-1Zr (d) 5Fe-1Zr[C]

### Fig.3 N<sub>2</sub> adsorption-desorption isotherms of the samples

### Fig.4 H<sub>2</sub>-TPR profiles of the samples

### Fig.5 CO<sub>2</sub>-TPD profiles of the samples

### Fig.6 XPS spectra of the samples

### Fig.7 Fe(2p) binding energy in 5Fe-1Zr-K

### Fig.8 C(1s) binding energy in 5Fe-1Zr-K

### Fig.9 Atomic Fe/Zr molar ratios on the sample surface

### Fig.10 CO<sub>2</sub> hydrogenation over 5Fe-1Zr-1K with time-on-stream

### Fig.11 $\alpha$ value of CO<sub>2</sub> hydrogenation over the catalyst samples

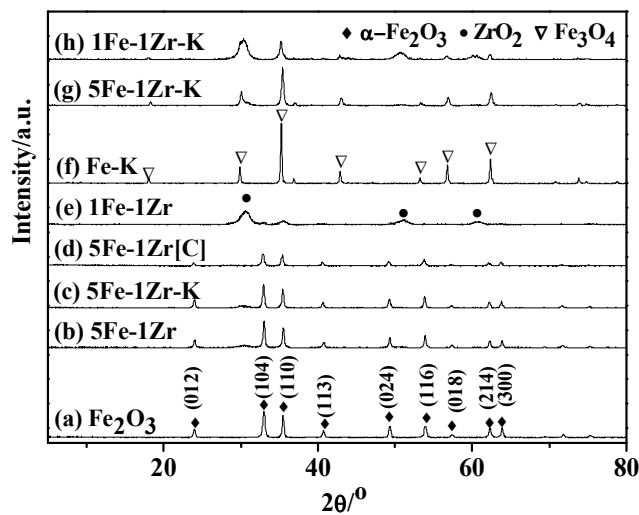


**Fig.1 XRD patterns of the samples**

(a)-(e): before reduction and reaction; (f)-(h): after reaction

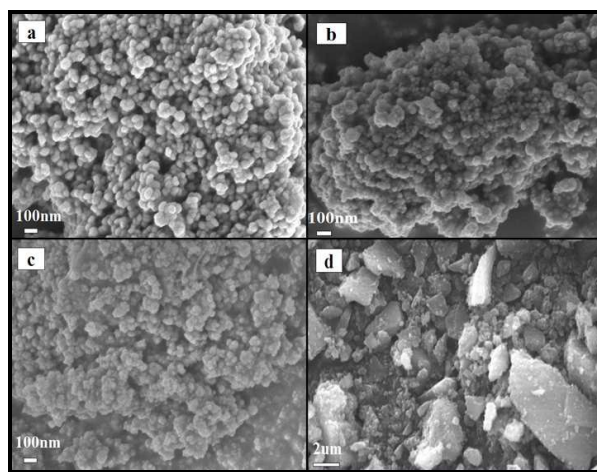


**Fig.2 SEM photographs of the samples**

(a)  $\text{Fe}_2\text{O}_3$  (b) 7Fe-1Zr (c) 5Fe-1Zr (d) 5Fe-1Zr[C]

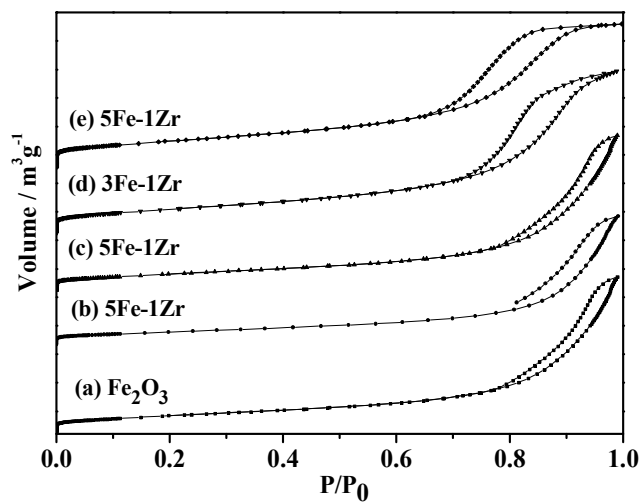


Fig.3 N<sub>2</sub> adsorption-desorption isotherms of the samples

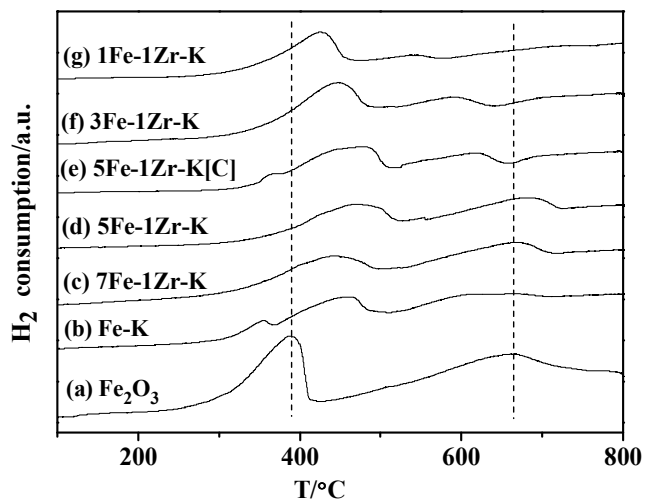


Fig.4 H<sub>2</sub>-TPR profiles of the samples

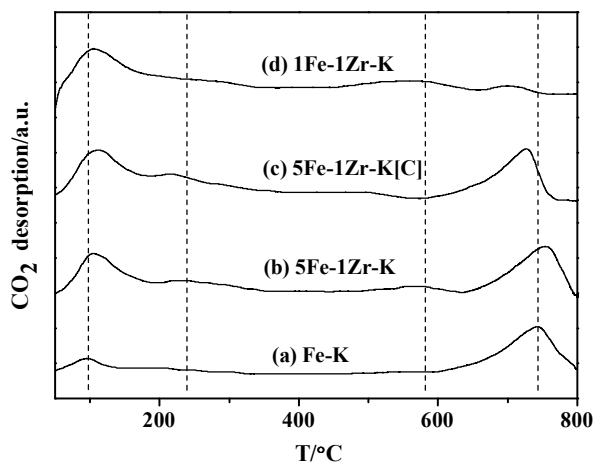


Fig.5 CO<sub>2</sub>-TPD profiles of the samples

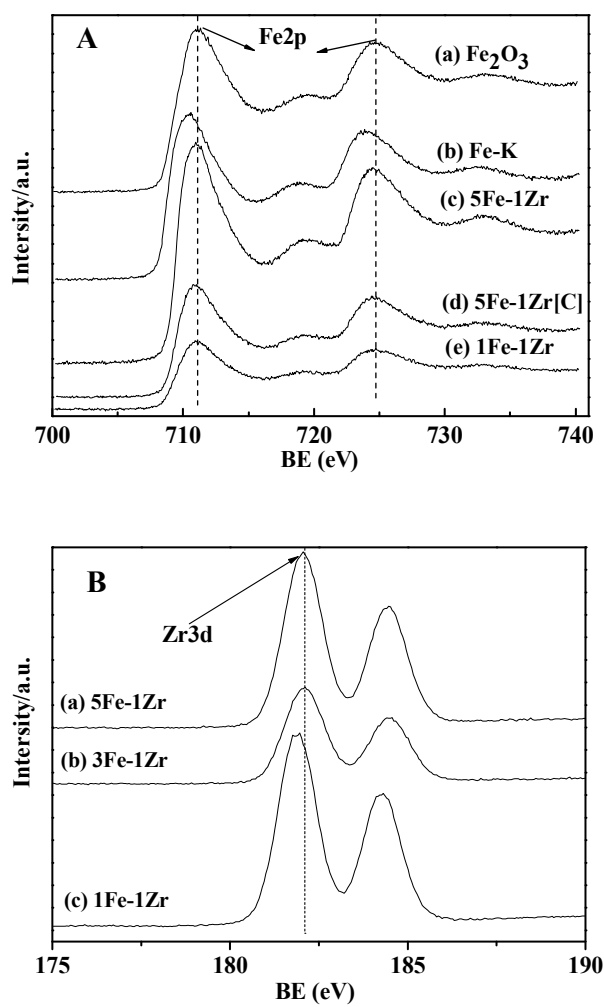


Fig.6 XPS spectra of the samples

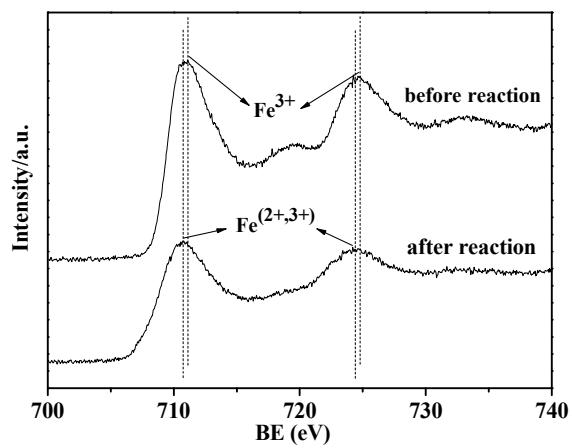


Fig.7 Fe (2p) binding energy in 5Fe-1Zr-K

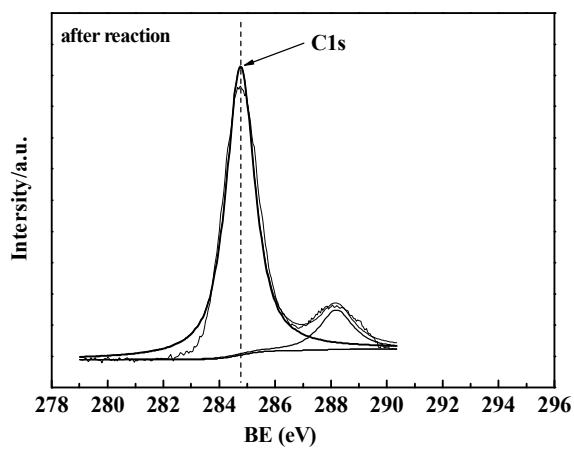
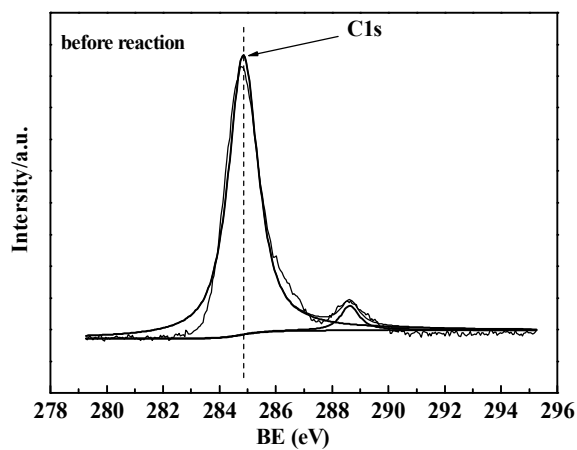


Fig.8 C(1s) binding energy in 5Fe-1Zr-K

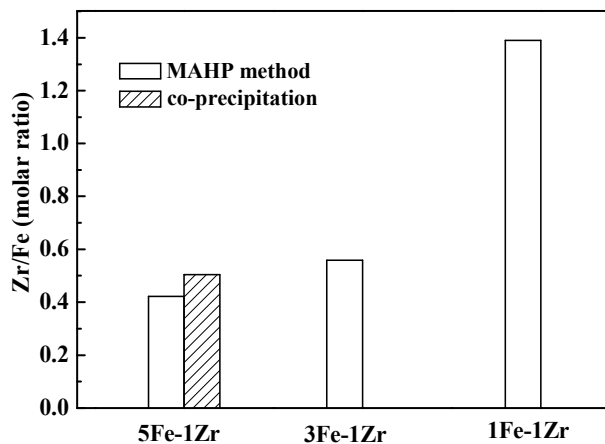


Fig.9 Atomic Zr/Fe molar ratios on the sample surface

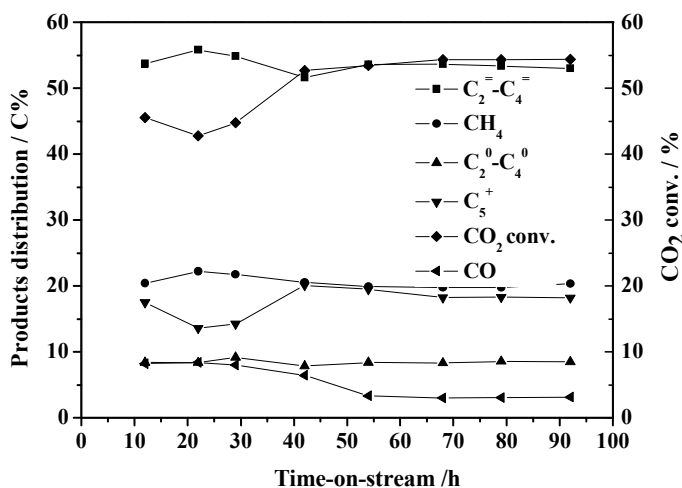


Fig.10 CO<sub>2</sub> hydrogenation over 5Fe-1Zr-1K with time-on-stream

Reaction conditions: H<sub>2</sub>/CO<sub>2</sub> = 3/1, GHSV = 1000 h<sup>-1</sup>, 2MPa, 320 °C

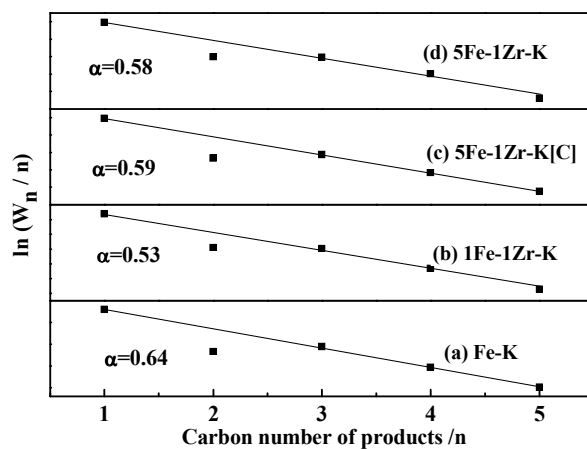


Fig.11  $\alpha$  value of CO<sub>2</sub> hydrogenation over the catalyst samples